Chemistry
A European
Journal

Chemistry Europe
European Chemical Societies Publishing

Accepted Article

Title: Recognition-Induced Enhanced Emission of Core-Fluorescent ESIPT-type Macrocycles

Authors: Paulina Jurek, Hanna Jędrzejewska, Michał F. Rode, and Agnieszka Szumna

To be cited as: *Chem. Eur. J.* **2022**, e202203116

Link to VoR: https://doi.org/10.1002/chem.202203116

WILEY-VCH

10.1002/chem.202203116

RESEARCH ARTICLE

WILEY-VCH

Recognition-Induced Enhanced Emission of Core-Fluorescent ESIPT-type Macrocycles

Paulina Jurek,[a] Hanna Jędrzejewska,[a] Michał F. Rode,[b] *and Agnieszka Szumna*[a]

[a] P. Jurek, Dr. Hanna Jędrzejewska, Prof. Agnieszka Szumna
Institute of Organic Chemistry Polish Academy of Sciences
Kasprzaka 44/52, 01-224 Warsaw, Poland
E-mail: agnieszka.szumna@icho.edu.pl

[b] Dr. M. F. Rode
Institute of Physics Polish Academy of Sciences
Aleja Lotników 32/46, 02-668 Warsaw, Poland
E-mail: mrode@ifpan.edu.pl

Supporting information for this article is given via a link at the end of the document.

Abstract: Core-fluorescent cavitands based on 2-(2′-resorcinol)benzimidazole fluorophores (**RBI**s) merged with the resorcin[4]arene skeleton were designed and synthesized. The cavitands, due to the presence of intramolecular hydrogen bonds and increased acidity, show excited state intramolecular proton transfer (ESIPT) and readily undergo deprotonation to form dianionic cavitands, capable of strong binding to organic cations. The changes in fluorescence are induced by deprotonation and binding events and involve huge Stokes shifts (due to emission from anionic double keto tautomers) and cation-selective enhancement of emission originating from the restriction of intramolecular motion (RIR) upon recognition in the cavity. *Ab initio* calculations indicate that the macrocyclic scaffold stabilizes the ground state tautomeric forms of the fluorophores that are not observed for non-macrocyclic analogs. In the excited state, the emitting forms for both macrocyclic scaffolds and non-macrocyclic analogs are anionic double keto tautomers, which are the result of excited state intramolecular proton transfer (ESIPT) or excited state double proton transfer (ESDPT).

Introduction

Fluorescence (FL), due to great sensitivity, superior temporal and spatial resolution, easy operation, biocompatibility, and high safety, is the most widely used optical signal for chemical sensing and biological imaging. For these applications, the Stokes shift and sensitivity of fluorophores to the stimulus are intrinsic features that determine their usability as emitting antennas. 2-(2′-hydroxyphenyl) benzimidazoles (**HBI**s, Fig. 1a) exhibit large Stokes shifts due to different absorbing and emitting forms (enol and keto tautomers, respectively) induced by excited state intramolecular proton transfer (ESIPT); **HBI** emissions are highly sensitive to the environment because of the presence of a rotatable bond between the phenol and benzimidazole parts. With these features, **HBI**s constitute great emitting antennas, provided that the binding is tuned by additional groups. Macrocyclic compounds, e. g. calixarene-type, are privileged scaffolds for selective binding because they provide a restrictive cavity to recognize guest molecules. Integration of various fluorescent units with these macrocycles is a common strategy for the construction of fluorescent molecular receptors, [1] whose selectivity and sensitivity depend crucially on the distance between signaling and binding sites, and typically, the closer distance provides stronger and more selective responses.[2]

In this paper, we present a new type of core-fluorescent macrocycles, tetrakis(2-benzimidazole)resorcin[4]arenes, (**T-RBI**s, **1a**-**1g** Fig. 1c). We hypothesize that (2-(2′-resorcinol)benzimidazole units, **RBI**s, resembling ESIPT-type fluorophores, will provide large Stokes shift and sensitivity to the surroundings, while their core positions enable selectivity and further increase sensitivity. As an additional advantage, we envisioned the possibility of recognition-induced enhanced emission (RIEE) due to the restriction of intramolecular rotation (RIR) caused by binding in the cavity. Here, we suggest that the RIR mechanism may also lead to in solution. Quite unexpectedly, further benefits of the designed molecules stemmed from the enhanced acidity that enabled selective deprotonation that turned on excited-state double proton transfer (ESDPT) which led to exceptionally large Stokes shifts of emission and greatly enhanced binding affinity.

It should be noted that macrocyclic compounds exhibiting either ESIPT or enhanced emission (mainly though processes involving aggregation-induced/enhanced emission, AIE, or AIEE) have been reported.[3, 4] However, to the best of our knowledge, macrocyclic compounds that exhibit a combination of these features and, particularly, macrocyclic compounds that respond to the recognition process by RIEE and ESIPT have not been known before.

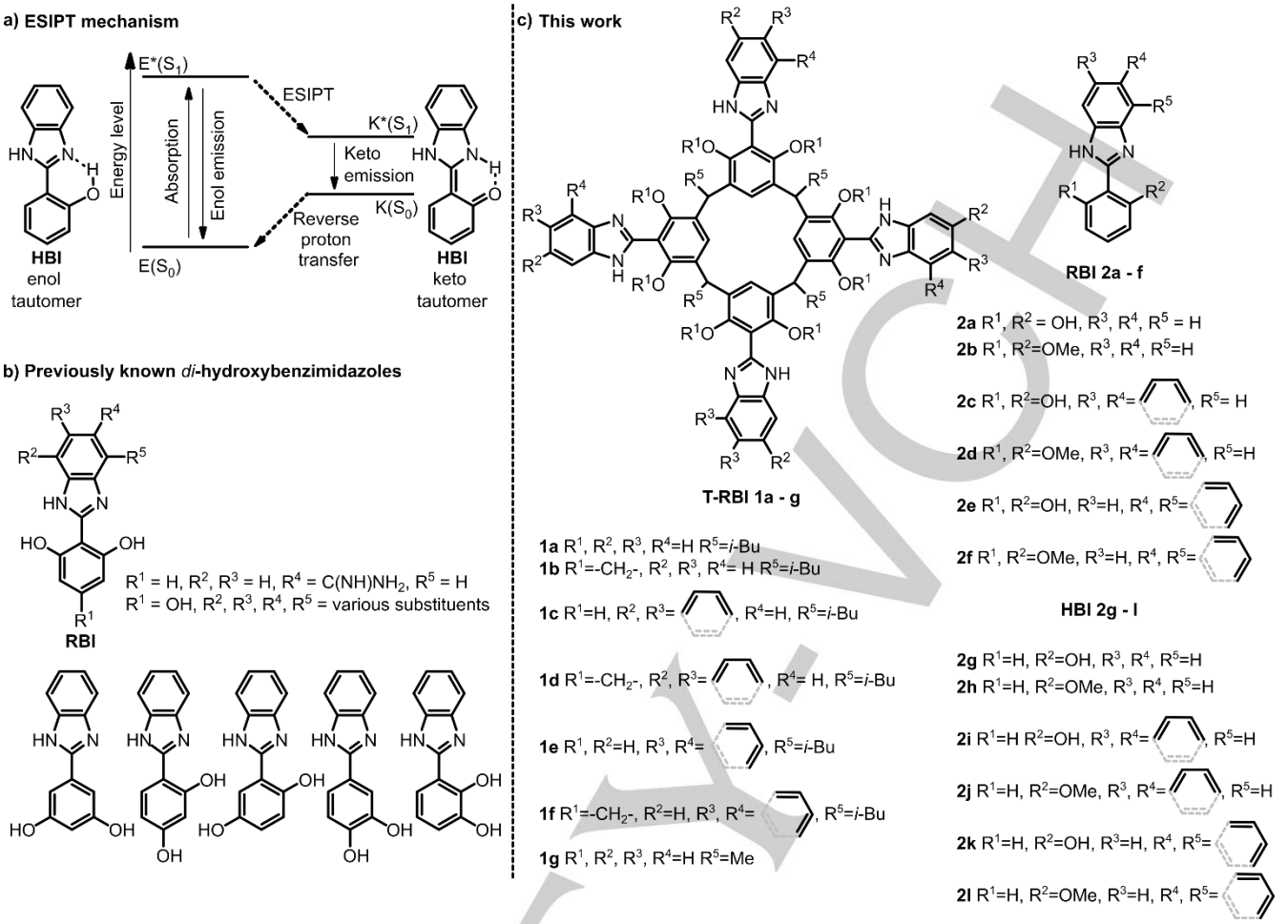

Figure 1. a) The mechanism of the ESPIT process; b) previously known, closely related derivatives, c) the compounds synthesized in this work (for synthesis see ESI).

Results and Discussion

Design, synthesis, and photophysical properties of cavitands

Resorcin[4]arenes feature two OH groups at each aromatic ring, therefore, we assumed that the formation of 2-(2′-resorcinol)benzimidazole units (**RBI**s) by attaching benzimidazoles to their walls, would create a system of hydrogen bonds that is similar to **HBI**s (Fig. 1a, c). Several non-macrocyclic *di*-hydroxybenzimidzoles are known so far (Fig. 1b), however, **RBI**s have only been tested for biological activity,[5] and their photophysical properties remain unknown. Photophysical properties have been only reported for *di*-hydroxybenzimidzoles with different substitution patterns (Fig. 1b, lower row).[6] To obtain tetrakis(2-benzimidazole)resorcin[4]arenes (**T-RBI**s), e.g. **1a**, reactions of resorcin[4]arene tetraaldehyde[7, 8] with 1,2-diaminobenzene were performed. The reaction under typical conditions (chloroform or ethanol, 2 days, Scheme S1) lead to imines as main products and subsequent oxidative ring-closing reaction (spontaneous for non-macrocyclic **HBI**s)[9] proved troublesome. Optimization of the condition (time, solvents, and addition of oxidants, Table S1) lead to the formation of **1a** as the main product (84% yield) in the reaction in EtOH, with $Na_2S_2O_5$ as an oxidant after 3 days. Reactions using I_2, H_2O_2 or DCQ gave either unreacted substrates or products of decomposition. The optimized conditions were employed for the synthesis of a set of macrocyclic **T-RBI**s involving OH-derivatives **1a** (84%)**, 1c** (89%), **1e** (91%), *O*-bridged derivatives **1b** (27%), **1d** (76%), **1f** (74%), non-macrocyclic **RBI**s **2a**-**2f** (41-97%) and **HBI**s **2g**-**2l** (52-79%). ^{1}H and ^{13}C NMR spectra of **1a, 1c,** and **1e** in [D_8]THF or [D_6]DMSO reveal their C_4 symmetry (Fig. 2e and SI). In [D_8]THF the signals of OH appear as two wide singlets at ca. 14.4 and 10.2 ppm. The signal at 10.2 ppm is typical for the OH group involved in an inter-unit H-bond, stabilizing C_4 symmetric vase conformations, while the signal at 14.4 ppm indicates involvement of the OH group in a strong intra-unit H-bond, being the prerequisite for efficient ESIPT. Indeed, the FL spectra confirm the presence of ESIPT for macrocyclic and non-macrocyclic derivatives featuring OH groups, e.g. **1a** and **2a** (the Stokes shifts of emission bands are ca. 170 nm, Figs. 2a, S74, S80) but not for the derivatives with OAlk groups, (e.g., exhibit Stokes shifts of ca. 50 nm for **2b**). A comparison of macrocyclic compounds with their non-macrocyclic analogs (e.g. **1a** and **2a**, Fig. 2a) reveals that the absorption and emission bands have

similar energies. The intensity of absorption bands (per unit) remains similar for macrocyclic compounds and non-macrocyclic analogs, while the emission quantum yield for macrocyclic compounds is reduced (Fig. S74-S91).

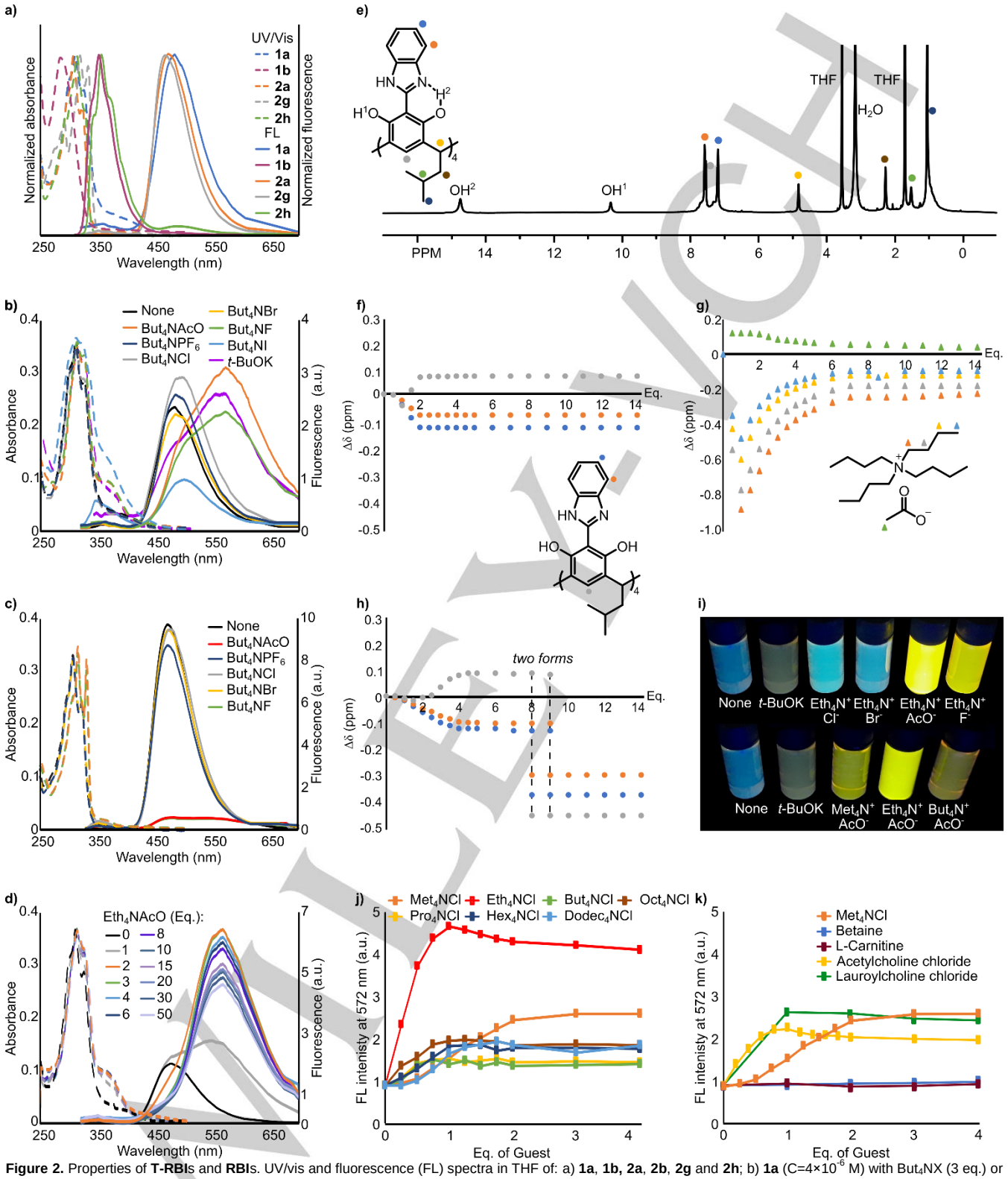

Figure 2. Properties of **T-RBI**s and **RBI**s. UV/vis and fluorescence (FL) spectra in THF of: a) **1a**, **1b, 2a**, **2b**, **2g** and **2h**; b) **1a** (C=4×10^{-6} M) with But$_4$NX (3 eq.) or *t*-BuOK (6 eq.); c) **2a** (C=1.6·10^{-5} M) with But$_4$NX (2 eq.); d) titration of **1a** (C=4·10^{-6} M) with Eth$_4$NAcO. e) ^{1}H NMR spectrum of **1a** (C=2×10^{-3} M, [D$_8$]THF). Chemical shift changes of various ^{1}H NMR signals during titrations of **1a** (C=2×10^{-3} M) with: f), g) But$_4$NAc; h) *t*-BuOK. i) Solutions of **1a** (C=8·10^{-4} M) with various guests (6eq. *t*-BuOK or 2eq. of Alk4NX, all in THF) under 356 nm light. j, k) Changes in FL intensity at 572 nm upon titration of [**1a**-2H]$^{2-}$ (**1a**, C=4×10^{-6} M + 6 eq. *t*-BuOK) with various guests in THF.

Recognition properties

Resorcin[4]arenes are known to bind cations in their electron-rich cavities[10] and/or complex anions between the arms or in their lower rims.[11] Both types of interactions can generate FL changes for **T-RBI**s. Initial screening of binding properties of **1a** was performed using various But_4NX salts in THF. The most pronounced changes in emission spectra were observed upon the addition of But_4NAcO and But_4NF, and, quite unexpectedly, these changes involved a large red shift of the emission band (+ 100 nm, Fig. 2b). The titration experiment shows that the maximum FL response is reached after 3 equivalents of the But_4NAcO or But_4NF added (Figs. S93e, f, S94e, f). The plausible hypothesis is that AcO^- and F^- cause deprotonation, forming a negatively charged cavitand. The hypothesis was confirmed by ^{1}H NMR titration of **1a** with But_4NAcO (Fig. 2f, g). Upon addition of But_4NAcO the signals of **1a** and AcO^- are shifted, and the changes in the slope of the titration curve for **1a** were observed at 2 eq. of But_4NAcO added, while for the signals of But_4N^+ the changes in the slope of the titration curve were observed at 1 eq. of But_4NAcO added. This is consistent with the process that involves di-deprotonation of **1a** by AcO^- to form [**1a**-2H]$^{2-}$, accompanied by binding of single But_4N^+ in the cavity. The ^{1}H NMR spectrum shows dynamically averaged C_{4v}-symmetry of [**1a**-2H]$^{2-}$ at 298 K. Upon lowering the temperature down to 222 K) the spectra reflect C_2 symmetry of [**1a**-2H]$^{2-}$ with two bridge signals, H_d (Fig. S117). The binding of But_4N^+ causes upfield shifts of all its aliphatic protons, but the most affected protons are those next to positively charged nitrogen, $^+NC\underline{H}_2$ (Fig. 2g). DOSY spectrum of the sample containing **1a** and 1 eq. of But_4NAcO, shows that in But_4N^+ diffuses at the same rate as [**1a**-2H]$^{2-}$ ($D=5.0\times10^{-10}m^2s^{-1}$), while AcOH exhibits higher diffusion rate ($D=20.0\times10^{-10}m^2s^{-1}$), characteristic for free species. Upon further addition of But_4NAcO (2 eq.), the D value for But_4N^+ increases, in agreement with dynamic equilibrium $But_4N^+_{bound}$ / $But_4N^+_{free}$. Thus, the DOSY results confirm that the addition of But_4NAcO to **1a** in THF results in the formation of complex [**1a**-2H]$^{2-}$ ⊃ Alk_4N^+, with AcO^- acting mainly as a base, which does not constitute an integral part of a complex. Notably, the deprotonation followed by complexation of the cation is very efficient - the response is linear and quantitative at 4×10^{-6} M concentrations (typically used for FL measurements).

Deprotonation of **1a** and other **RBI**s was further studied using various bases. It was found that the acidity of **RBI**s (Figs. S108, S109, S110) is greatly increased in comparison to **HBI**s (Figs. S112, S113, S114) or unsubstituted resorcinol (Fig. S115). For **1a** at a concentration of 4×10^{-6} M in THF deprotonation requires 3 eq. But_4NAcO or But_4N^+F and 6 eq. of *t*-BuOK (Figs. 2b, S93, S94) while Et_3N (Fig. S92a, b) does not cause any changes. Di-deprotonation of **1a** to [**1a**-2H]$^{2-}$, irrespective of the type of the base used, is accompanied by the formation of an absorption shoulder at 365 nm, quenches emission at 470 nm and leads to the formation of a very weak and broad emission that spans from 450 to 700 nm (Fig. 2b). Further addition of the bases does not induce changes, indicating that higher deprotonation states are not accessible at this concentration. However, at concentration 2×10^{-3} M (used for NMR titrations) and *t*-BuOK as a base two deprotonation steps are observed (Fig. 2g). [**1a**-2H]$^{2-}$ dominates between 3 and 6 eq. of *t*-BuOK. The second form was obtained after the addition of 8 eq. of *t*-BuOK (Fig. 2h) and has a well-resolved ^{1}H NMR spectrum reflecting the C_{4v} symmetry of the molecule, therefore it was attributed to [**1a**-4H]$^{4-}$.

It is expected that recognition of the guest in the cavity should lead to restriction of intramolecular motion and increase of FL intensity. To test this hypothesis, the guests bearing ammonium cationic groups of different sizes were added to samples containing [**1a**-2H]$^{2-}$ in THF (generated by using 6 eq. of *t*-BuOK, Fig. 2j, k). Indeed, the cation-dependent enhancement of emission was observed. The largest increase in FL intensity was observed after the addition of Eth_4NCl, while larger and smaller cations (Pro_4N^+, But_4N^+, Hex_4N^+, Oct_4N^+, $Dodec_4N^+$, Met_4N^+) exert considerably smaller effects (Fig. 2j). For Eth_4NCl the increase of FL is linear suggesting high K_{ass} ($>10^7$ M^{-1}) and enabling quantitative detection of this cation. Although numerous receptors responding to Alk_4NX salts are known,[10,12] the size-dependent selectivity and FL response involving large Stokes shift and intensity enhancement is unprecedented. Importantly, [**1a**-2H]$^{2-}$ binds also biologically active choline derivatives, however, remains insensitive to analytes bearing structurally identical trimethylammonium terminal group, but having a zwitterionic character (betaine and L-carnitine), pointing out to the crucial role of electrostatic interactions in the binding event (Fig. 2k).

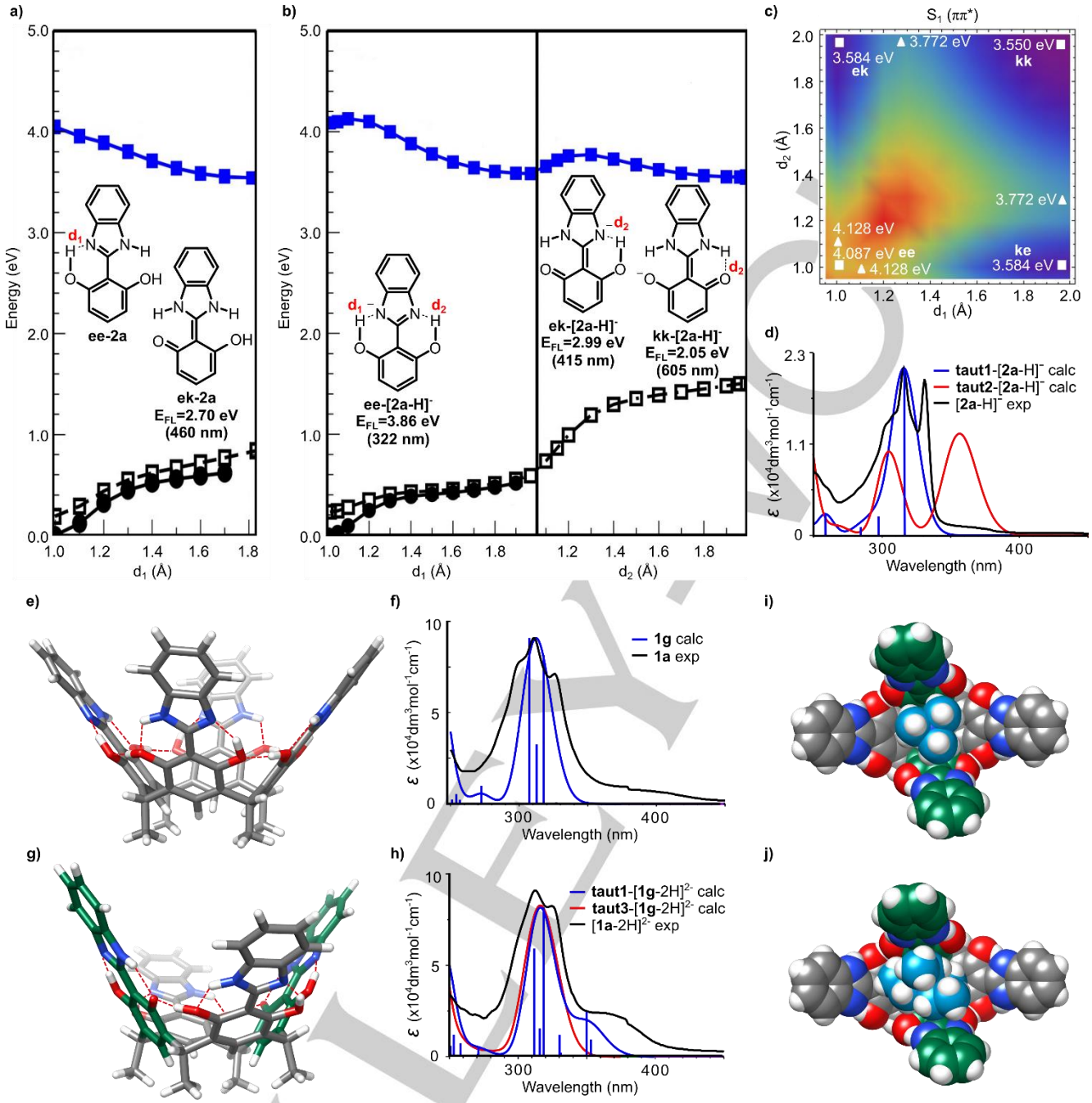

Figure 3. Calculations of photophysical and binding properties of **2a** and **2g** in neutral and anionic forms. Minimum potential energy profiles of the ground (S_0) and the lowest ππ* excited singlet (S_1) states as a function of proton-transfer coordinates for: a) **2a**; b) [**2a**-H]$^{\cdot}$ c) 2D minimum potential energy surface for S_1 (ππ*) state as a function of two OH distances for [**2a**-H]$^{\cdot}$ (MP2 for S_0 and CC2/cc-pVDZ for S_1 in a vacuum, ● S_0, ■ lowest singlet state S_1, □ S_0 computed using the geometry of S_1). d) Comparison of experimental and calculated UV/Vis spectra for [**2a**-H]$^{\cdot}$. e) Energy-optimized structure of **2g** and f) comparison of calculated UV/Vis spectrum of **2g** and **2a.** g) Energy-optimized lowest energy tautomer of [**1g**-2H]$^{2-}$ and h) comparison of calculated UV/Vis spectra with the experimental spectrum of [**1a**-2H]$^{2-}$**.** Energy-optimized structures of: i) [**1g**-2H]$^{2-}$ ⊃ Met_4N^+ , and j) [**1g**-2H]$^{2-}$ ⊃ Eth_4N^+ [**1g**-2H]$^{2-}$ (grey – neutral units, green – anionic units, all geometry optimizations for cavitands and all UV spectra at S_0 state by TD-DFT WB97XD/dgdzvp in THF).

The hypothesis that deprotonation and size-dependent cation binding are both crucial for the generation of the new FL band with the increased intensity was verified by a series of control experiments. The *O*-bridged derivative **1b**, which is not capable of deprotonation does not show notable changes in the FL or NMR spectra upon the addition of various guests (Fig. S98-S102). Non-macrocyclic derivative, **2a**, undergoes quantitative monodeprotonation upon addition of But_4NAcO or *t*-

BuOK, which is accompanied by quenching of emission at 470 nm and formation of very weak 570-670 nm emission band with cation-independent intensity (Fig. 2c, S108-S110). Titration of **1a** with But_4NAcO in [D_6]DMSO (the solvent which eliminates complexation in the cavity and diminishes ion-pairing) monitored by ^1H NMR reveals di-deprotonation (Fig. S120) and lack of cation's complexation ($|\Delta\delta| \leq 0.2$ ppm for But_4N^+, Eth_4N^+ or Met_4N^+). Accordingly, the titration of **1a** with But_4NAcO in DMSO monitored by UV and FL revealed quenching of the emission band at 470 nm and formation of a new wide emission at 570 nm, in agreement with deprotonation (however, the deprotonation process requires more base than the analogous process in THF, Figs. S93e, f, S96c, d), that has a low cation-insensitive intensity in DMSO. These experiments confirm that the recognition of cations, which is unique for the macrocyclic skeleton is responsible for the enhancement of emission.

Further experiments indicate that not only the type of the guest but also the geometrical parameters of the cavity exert large effects on binding and emission. For example, **1c**, which has a deeper cavity than **1a**, exhibits similar di-deprotonation characteristics but no response to the size of Alk_4N^+ (emission intensity remains low for all Alk_4NX, Fig. S104, S105). Apparently, a larger cavity is less tightly filled with the cations and therefore the RIR mechanism is less efficient. For **1e**, with the cavity that is distorted by conformational effects the low-intensity red-shifted emission band emerges upon addition of 2 or more eq. of Alk_4NAcO containing small cations, while for larger cations the blue-shifted FL band with low intensity emerges (Fig. S106). These experiments illustrate the high sensitivity and selectivity of the emission to the recognition process and geometrical parameters.

Calculations of photophysical properties and modes of interactions

The unusually large Stokes shift, observed upon deprotonation of **RBI**s and **T-RBI**s, has not been known before for any of the **HBI** derivatives: either having a single *ortho*-OH group (e.g. **HBI** shows blue-shift after deprotonation according to the previous reports,[13] confirmed also in THF, Fig. S111-S114) or for analogs with two OH groups at different positions (e.g. 2-(2′,4′-dihydroxyphenyl)benzimidazole exhibits quenching of the fluorescence upon pH increase[14]). The origins of such large Stokes shifts for **RBI**s were examined by theoretical *ab initio* calculations for **2a** and [**2a**-H]$^-$ in the ground state, S_0, and in the excited state, S_1 (MP2 for, S_0, and CC2 for S_1, in vacuum), and analysis of the minimum potential energy profiles along the proton transfer OH stretching coordinates (crucial for ESIPT) and torsional angles (important for RIR mechanism). Based on the optimized structures of the monomers the models of macrocyclic tetramers: neutral **1g** (a homolog of **1a** with CH_3 alkyl lower rim tail), anionic [**1g**-2H]$^{2-}$ and complexes [**1g**-2H]$^{2-}$ ⊃ Met_4N^+ and [**1g**-2H]$^{2-}$ ⊃ Eth_4N^+ were constructed, optimized (S_0) and their absorption spectra were calculated (TD-DFT WB97XD/dgdzvp).[15]

For neutral **2a** the lowest energy structure in the S_0 state is planar enol-enol tautomer, **ee-2a,** which is stabilized by two intramolecular hydrogen bonds: OH···N and NH···O (Fig. 3a). Photoexcitation of **ee-2a** populates the ππ* excited state S_1, **ee-2a**(S_1) (see Table S2) and molecule then evolves along the barrierless intramolecular proton transfer (ESIPT) pathway towards the planar enol-keto tautomer, **ek-2a** (S_1), which is also stabilized by two hydrogen bonds. According to CC2/cc-pVDZ calculations, **ek-2a** (S_1) emits at 2.70 eV (460 nm) and this value agrees well with the experimentally observed emission at 480 nm (2.59 eV, in THF). After the emission, the barrierless back proton transfer occurs in the S_0 state, repopulating the **ee-2a** form. The non-planar conformations of **2a** either in the S_0 or S_1 state are higher in energy (much larger in the S_0 than the S_1 state, Fig. S124, S125) due to double bond interunit connection.

Macrocycle **1g,** constructed by bridging four **ee-2a** units (lowest energy tautomer of **2a**), has all hydrogen bond donors and acceptors saturated and its vase conformation is stabilized by four hydrogen bonds between the units (Fig. S129). The geometry optimization retains C_4 symmetry and the vase conformation of **1g** with a hydrogen bond system that facilitates ESIPT (Fig. 3e). The model agrees with ^{13}C NMR spectra that show C_4 symmetry of **1a** and demonstrate **ee** tautomeric forms of all units. The calculated UV spectrum for this model agrees well with the experimental UV spectrum of **1a** in THF (Fig. 3f).

For the anionic monomer, [**2a**-H]$^-$, in the S_0 state the lowest energy tautomer is planar **ee-**[**2a**-H]$^-$, with protons located at oxygen atoms and forming two intramolecular hydrogen bonds: $OH_1\cdots N_1$ and $OH_2\cdots N_2$ (Fig. 3b). The **ek-**[**2a**-H]$^-$ tautomer (one proton located at the oxygen atom, two intramolecular hydrogen bonds: O···HN and OH···N), is unstable. Upon photoexcitation of **ee-**[**2a**-H]$^-$ to the S_1 (ππ*) state, both single and double ESIPT processes are possible leading to the tautomers: **ek-**[**2a**-H]$^-$(S_1) and **kk-**[**2a**-H]$^-$(S_1), respectively. The lowest S_1 state energy tautomer is **kk-**[**2a**-H]$^-$(S_1) with the emission energy E_{FL} of 2.05 eV (605 nm), while the emission from **ek-**[**2a**-H]$^-$(S_1) has the energy of 2.99 eV (415 nm). These calculations suggest that the experimentally observed emission (570 nm, 2.18 eV) originates from **kk-**[**2a**-H]$^-$ the tautomeric form that is a result of the excited-state double-proton transfer (ESDPT). The analysis of the 2D energy surface as a function of the two OH distances indicates that ESDPT proceeds asynchronously and both steps are hindered by low-energy barriers (+0.041 eV and +0.188 eV, respectively, Fig. 3c). ESDPT as a rare photophysical process can lead up to three emission bands with the large Stokes shifts (observed also here). It was previously reported for quinoline–benzimidazoles,[16] 3-hydroxy-picolinic acid,[17] bipyridine-diols,[18] benzoxazole-thiophenediol,[19] 2-hydroxyphenyl-triazoles.[20] An intermolecular ESDPT was also induced by guest binding in a bis-acridine supramolecular receptor.[21] However, ESDPT–type fluorophores have not been previously incorporated into a macrocyclic structure or served as sensitive probes for recognition.

Di-deprotonated macrocycle [**1g**-2H]$^{2-}$ was constructed using units **2a** and [**2a**-H]$^-$ positioned alternatively. Considering the number of possible tautomeric forms, conformations, and hydrogen bonding patterns, the prediction of the structure of [**1g**-2H]$^{2-}$ is challenging. We have constructed 16 tautomers of [**1g**-2H]$^{2-}$ with C_2 symmetry (suggested by NMR) and optimized their geometries (DFT B3LYP/dgdzvp, Table S6, Fig. S130). In none of the structures, the fully complementary system of hydrogen bonds is possible. The lowest energy structure (among the tested ones) is **taut1-**[**1g**-2H]$^{2-}$ with neutral units as **ee** tautomers and anionic units as **ek** tautomers (Fig. 3g). Thus, the calculations suggest that anionic units stabilized within a macrocyclic scaffold have different tautomeric forms (**ek**) than the lowest energy tautomer, found for monomeric [**2a**-H]$^-$ (**ee**).

Taut3-[**1g**-2H]$^{2-}$ with anionic unit as **ee** tautomer has energy higher by 41.4 kJ/mol. Most likely this difference originates from stabilization of phenolate negative charge by hydrogen bonds from the neighboring neutral unit. Different tautomeric forms of anionic units of the monomer and in the macrocycle were further confirmed by comparison of calculated and experimental UV spectra. For the monomer, the experimental UV spectrum [**2a**-H]$^-$ is reproduced well with the calculated spectrum of **ee-**[**2a**-H]$^-$ but not **ek-**[**2a**-H]$^-$ (Fig. 3d) while for the macrocycle the experimental UV spectrum of [**1a**-2H]$^{2-}$ is reproduced well with the calculated spectrum for **taut1-**[**1g**-2H]$^{2-}$ but not **taut3-**[**1g**-2H]$^{2-}$ (Fig. 3h). Despite the differences in the tautomeric forms in the S_0 state, the emission energy for monomer [**2a**-H]$^-$ and macrocycle [**1a-**2H]$^{2-}$ is similar, indicating that the emitting tautomers in the S_1 state are the same - **kk**. This tautomer is the result of the excited-state double-proton transfer (ESDPT) for [**2a**-H]$^-$ while for [**1a-**2H]$^{2-}$ only single excited state proton transfer (ESIPT) occurs because the first proton transfer proceeds already in the ground state induced by intramolecular interactions.

The lowest energy structure, **taut1-**[**1g**-2H]$^{2-}$, has a C_2-symmetrical vase conformation with anionic units positioned more vertically than the neutral units (the opposite arrangement is higher in energy by 1.4 kJ/mol (**taut1a-**[**1g**-2H]$^{2-}$). Such a conformation possesses a cavity that is perfectly preorganized to bind cationic guests in proximity to negatively charged walls. The optimized models of the complexes [**1g**-2H]$^{2-}$ ⊃ Met_4N^+ (Fig. 3i) and [**1g**-2H]$^{2-}$ ⊃ Eth_4N^+ (Fig. 3j) show the size of Eth_4N^+ is optimal for the binding in the cavity and the restriction of intramolecular rotation (RIR) about phenolate-benzimidazole bonds of the anionic units. These features are responsible for strong binding and enhancement of emission. In the case of Met_4N^+, RIR is less effective due to the smaller guest's size and this conclusion is in line with the experimentally observed weaker enhancement of emission.

Conclusion

In conclusion, we have designed and synthesized new core-fluorescent cavitands, **T-RBI**s, based on 2-(2′-resorcinol)benzimidazole fluorophores (**RBI**s). **T-RBI**s show effective ESIPT resulting in a red shift of their emission bands. Moreover, they undergo selective deprotonation to form dianionic cavitands capable of very strong binding of alkylammonium cations. Size-selective FL response generated during this process involves a further red shift of emission and its enhancement. Detailed analysis by computational methods revealed that the mechanism of the response involves the emission from the double keto forms (causing large Stokes shifts) and recognition-induced restriction of intramolecular motion due to complexation in the cavity (causing FL enhancement). The FL enhancement is cation-selective and reflects the size match between the cation and the cavity.

The generation of FL response by core-fluorescent macrocycles through the recognition-induced restriction of intramolecular motion proved to be highly selective and sensitive, which opens the way for the construction of other turn-on type receptors based on similar assumptions. Additionally, the newly revealed photophysical properties of **RBI**s, exhibiting large, protonation-dependent Stokes shifts, together with their relatively easy synthesis make them great candidates as new ESIPT or ESDPT fluorophores for various applications in supramolecular chemistry, biology, and materials science.

Experimental Section

Synthesis of 1a: The synthesis was based on an optimized general procedure (SI). Tetraformylresorcin[4]arene **S4** (100 mg, 0.106 mmol) and 1,2-diaminobenzene derivative (45.9 mg, 0.426 mmol) were dissolved in ethanol (5 ml), then $Na_2S_2O_5$ solution (0.34 ml, 2.85 M) was added. The reaction mixture was stirred for 3 days at 80°C. Then 1M solution of HCl (2.12 ml) was added. The precipitate was collected and washed with water and diethyl ether. Product **1a** was obtained as orange solid, yield 78% (98 mg, 0.083 mmol). **^{1}H NMR** (600 MHz, [D_6]DMSO, 298 K) δ=7.80 (s, 1H), 7.69 (d, *J*=6.2, 2H), 7.28 (d, *J*=6.1 Hz, 2H), 4.74 (t, *J*=7.8 Hz, 1H), 2.35 (t, *J*=7.1 Hz, 2H), 1.57–1.49 (m, 1H), 1.04 (d, *J*=6.6 Hz, 6H). **^{13}C NMR** (150 MHz, [D_6]DMSO, 298 K) δ=153.2, 150.3, 134.1, 127.3, 124.2, 123.1, 114.5, 100.3, 41.2, 31.2, 26.2, 22.8. **Diffusion coefficient (DOSY)** 1.6×10^{-10} m^2s^{-1} in [D_6]DMSO, diameter 1.25 nm. **HRMS (ESI):** m/z calcd for $C_{72}H_{72}N_8O_8$+H:1177.5551[*M*+H]$^+$; found 1177.5566.

Synthesis of 2a: The synthesis was based on an optimized general procedure (SI). 2,6-dihydroxybenzaldehyde[22] (11.1 mg, 0.08 mmol) and 1,2-diaminobenzene (8.7 mg, 0.08 mmol.) were dissolved in ethanol (1 ml), then $Na_2S_2O_5$ solution (0.07 ml, 2.85 M) was added. The reaction mixture was stirred for 3 days at 80°C. Then 1M solution of HCl (0.5 ml) was added. The precipitate was collected and washed with water and diethyl ether. Product **2a** was obtained as brown solid was obtained, yield 66% (12 mg, 0.053 mmol). **^{1}H NMR** (500 MHz, [D_6]DMSO, 298 K) δ=12.79 (brs, 1H, NH), 7.82–7.81 (m, 2H), 7.42–7.40 (m, 2H), 7.28 (t, *J*=8.26 Hz, 1H), 6.60 (d, *J*=8.2 Hz, 2H). **^{13}C NMR** (125 MHz, [D_6]DMSO, 298 K) δ=158.2, 147.2, 133.6, 124.2, 114.4, 107.0, 99.3. **HRMS (ESI):** m/z calcd for $C_{13}H_{10}N_2O_2$+H: 227.0821[*M*+H]$^+$; found 227.0811.

General procedure for UV and FL titrations: To the solution of **1a** ($C=4\times10^{-6}$ M, 0.00001 mmol) in THF or DMSO (2.5 ml) a solution containing a guest (C=0.001 M, 0.005 mmol) and the macrocycle ($C=4\times10^{-6}$ M, 0.00002 mmol) in THF or DMSO (5 ml) was added. UV and FL spectra were recorded at room temperature on U-1900 Spectrophotometer (UV/Vis) and F-7000 FL Spectrophotometer. Excitation was at isosbestic points (UV spectra) and experiments were repeated twice.

General procedure for ^{1}H NMR titrations: To the solution of **1a** (C=0.002 M, 0.003 mmol) in [D_8]THF or [D_6]DMSO (0.5 ml) a solution containing a guest (C=0.045 M, 0.045 mmol) and the macrocycle (C=0.002 M, 0.001 mmol) in [D_8]THF or [D_6]DMSO (1 ml) was added. ^{1}H NMR spectra were recorded at 303 K using Bruker 400 MHz.

Acknowledgements

This work was supported by the National Science Centre (PJ, HJ and AS from OPUS 2017/25/B/ST5/01011). The calculations were performed at the Wroclaw Centre for Networking and Supercomputing (grant no. 299) and the PL-Grid infrastructure. We are grateful to Dr. Piotr Cmoch for measuring NMR spectra.

Keywords: fluorescence • macrocycles • calixarenes • ESIPT • complexation

[1] a) R. Kumar, A. Sharma, H. Singh, P. Suating, H. S. Kim, K. Sunwoo, I. Shim, B. C. Gibb, J. S. Kim, *Chem. Rev.* **2019**, *119*, 9657-9721; b) S.K. Kim, B.-S. Moon, J. H. Park, Y. I. Seo, H. S. Koa, Y. J. Yoon, K. D. Lee,

J. Yoon, *Tetrahedron Lett.* **2005**, *46*, 6617-6620; c) I. Aoki, T. Sakaki, S. Tsutsui, S. Shinkai, *Tetrahedron Lett.* **1992**, *33*, 89-92; d) A. Szafraniec, W. Iwanek, *Int. J. Mol. Sci.* **2020**, *21*, 6160.

[2] a) Y. Kubo, K. Tsuruzoe, S. Okuyama, R. Nishiyabua, T. Fujihara, *Chem.Commun.* **2010**, *46*, 3604-3606; b) K. Otsuka, T. Kondo, R. Nishiyabu, Y. Kubo, *J. Org. Chem.* **2013**, *78*, 5782-5787; c) O. B. Berryman, A. C. Sather, J. Rebek, Jr., *Org. Lett.* **2011**, *13*, 5232-5235; d) P. Kumar, P. Venkatakrishnan, *Org.Lett.* **2018**, *20*, 1295-1299; e) S. Tashiro, T. Umeki, R. Kubota, M. Shionoya, *Chem. Sci.* **2018**, *9*, 7614-7619; f) Nitisha, P. Venkatakrishnan, *J. Org. Chem*. **2019**, *84*, 10679-10689; g) P. Kumar, P. Venkatakrishnan, *Eur. J. Org. Chem.* **2019**, 7787-7799; h) A. Kumar, P. Venkatakrishnan, *Asian J. Org. Chem*. **2021**,*10*,1390-1394.

[3] H.-T. Feng, Y.-X. Yuan, J.-B. Xiong, Y.-S. Zheng, B. Z. Tang, *Chem. Soc. Rev.* **2018**, *47*, 7452-7476.

[4] H. Qu, X. Tang, X. Wang, Z. Li, Z. Huang, H. Zhang, Z. Tian, X. Cao, *Chem. Sci.* **2018**, *9*, 8814-8818.

[5] a) J. Matysiak, A. Skrzypek, M. Karpińska, K. Czarnecka, P. Szymański, M. Bajda, A. Niewiadomy, *Biomolecules* **2019**, *9*, 870; b) A. Baldisserotto, M. Demurtas, I. Lampronti, M. Tacchini, D. Moi, G. Balboni, S. Pacifico, S. Vertuani, S. Manfredini, V. Onnis, *Bioorg. Chem.* **2020**, *94*, 103396; c) K. M. Khan, Z. Shah, V. U. Ahmad, N. Ambreen, M. Khan, M. Taha, F. Rahim, S. Noreen, S. Perveen, M. I. Choudhary, W. Voelter, *Bioorg. Med. Chem.* **2012**, *20*, 1521-1526; d) B. A. Bhongade, V. V.Gouripur, A. K.Gadad, *Bioorg. Med. Chem.* **2005**, *13*, 2773-2782; e) E. Verner, B. A. Katz, J. R. Spencer, D. Allen, J. Hataye, W. Hruzewicz, H. C. Hui, A. Kolesnikov, Y. Li, C. Luong, A. Martelli, K. Radika, R. Rai, M. She, W. Shrader, P. A. Sprengeler, S. Trapp, J. Wang, W. B. Young, R. L. Mackman, *J. Med. Chem.* **2001**, *44*, 2753-2771; f) M. M. Karpińska, J. Matysiak, A. Niewiadomy, *Arch. Pharm. Res.* **2011**, *34*, 1639-1647.

[6] a) A. Bino, A. Baldisserotto, E. Scalambra, V. Dissette, D. E. Vedaldi, A. Salvador, E. Durini, S. Manfredini, S. Vertuani, *J. Enzyme Inhib. Med. Chem.* **2017**, *32*, 527-537; b) A. Tavman, A. Çinarli, D. Gürbüz, A. S. Birteksöz, *J. Iran. Chem. Soc.* **2012**, *9*, 815-825; c) F. Han, X. Zhang, J. Zhang, Y. Wei, X. Zhang, W. Huang, H. Xu, *Chem. Commun.* **2016**, *52*, 5183-5186; d) D. Wu, Y. Zhao, K. Zeng, G. Yang, *J. Polym. Sci., Part A: Polym. Chem.* **2012**, *50*, 4977-4982.

[7] M. Grajda, M. Wierzbicki, P. Cmoch, A. Szumna, *J. Org. Chem.* **2013**, *78*, 11597-11601.

[8] H. Jędrzejewska, M. Wierzbicki, P. Cmoch, K. Rissanen, A. Szumna, *Angew. Chem. Int. Ed.* **2014***, 53,* 13760-13764.

[9] a) D. Maity, M. G. B. Drew, J. F. Godsell, S. Roy, G. Mukhopadhyay, *Transit. Met. Chem.* **2010**, *35*, 197-204; b) R. K. Bagautdinova, L. K. Kibardina, A. R. Burilov, A. G. Strelnik, M. A. Pudovik, *Chem. Heterocycl.* **2020**, *56*, 326-330; c) M.-Y. Duan, J. Li, Y. Xi, X.-F. Lü, J.-Z. Liu, G. Mele, F.-X. Zhang, *J. Coord. Chem*. **2010**, *63*, 90-98.

[10] a) N. K. Beyeh, A. Valkonen, K. Rissanen, *Supramol. Chem.* **2009**, *21*, 142-148; b) N. K. Beyeh, K. Rissanen, *Isr. J. Chem.* **2011**, *51*, 769-780; c) H. Mansikkamäki , M. Nissinen, K. Rissanen, *Chem. Commun.* **2002**, 1902-1903; d) H. Mansikkamäki, M. Nissinen, C. A. Schalley, K. Rissanen, *New J. Chem.* **2003**, *27*, 88-97; e) N. K. Beyeh, D. P. Weimann, L. Kaufmann, C. A. Schalley, K. Rissanen, *Chem. Eur. J.* **2012**, *18*, 5552-5557; f) N. K. Beyeh, M. Göth, L. Kaufmann, C. A. Schalley, K. Rissanen, *Eur. J. Org. Chem.* **2014**, 80-85.

[11] a) M. Chwastek, P. Cmoch, A. Szumna, *Angew. Chem., Int. Ed.* **2021**, *60*, 4540-4544; b) M. Chwastek, P. Cmoch, A. Szumna, *J. Am. Chem. Soc.* **2022**, *144*, 5350-5358; c) E. R. Abdurakhmanova, P. Cmoch, A. Szumna, *Org. Biomol. Chem.* **2022**, *20*, 5095-5103.

[12] a) S. Bartoli, S. Roelens, *J. Am. Chem. Soc.* **2002**, *124*, 8307-8315; b) F. Hof, L. Trembleau, E. C. Ullrich, J. Rebek, Jr., *Angew. Chem. Int. Ed.* **2003**, *42*, 3150-3153; c) R. Carrillo, M. J. Hynes, V. S. Martín, T. Martín, F. Pinacho Crisóstomo, *Org. Lett.* **2015**, *17*, 2912-2915; d) B. Bibal, *Supramol. Chem.* **2018**, *30*, 243-254.

[13] S. Sahu, M. Das, G. Krishnamoorthy, *Phys. Chem. Chem. Phys.* **2016**, *18*, 11081-11090.

[14] V. S. Patil, V. S. Padalkar, A. B. Tathe, V. D. Gupta, N. Sekar, *J. Fluoresc.* **2013**, *23*,1019-1029.

[15] M. J. Frisch, G. W. Trucks, H. B. Schlegel, G. E. Scuseria, M. A. Robb, J. R. Cheeseman, G. Scalmani, V. Barone, G. A. Petersson, H. Nakatsuji, X. Li, M. Caricato, A. V. Marenich, J. Bloino, B. G. Janesko, R. Gomperts, B. Mennucci, H. P. Hratchian, J. V. Ortiz, A. F. Izmaylov, J. L. Sonnenberg, D. Williams-Young, F. Ding, F. Lipparini, F. Egidi, J. Goings, B. Peng, A. Petrone, T. Henderson, D. Ranasinghe, V. G. Zakrzewski, J. Gao, N. Rega, G. Zheng, W. Liang, M. Hada, M. Ehara, K. Toyota, R. Fukuda, J. Hasegawa, M. Ishida, T. Nakajima, Y. Honda, O. Kitao, H. Nakai, T. Vreven, K. Throssell, J. A. Montgomery, Jr., J. E. Peralta, F. Ogliaro, M. J. Bearpark, J. J. Heyd, E. N. Brothers, K. N. Kudin, V. N. Staroverov, T. A. Keith, R. Kobayashi, J. Normand, K. Raghavachari, A. P. Rendell, J. C. Burant, S. S. Iyengar, J. Tomasi, M. Cossi, J. M. Millam, M. Klene, C. Adamo, R. Cammi, J. W. Ochterski, R. L. Martin, K. Morokuma, O. Farkas, J. B. Foresman, and D. J. Fox, *Gaussian 16,* Revision C.01, Gaussian, Inc., Wallingford CT, **2016**.

[16] G. Kumar, K. Paul, V. Luxami, *New J. Chem.* **2020**, *44*, 12866-12874.

[17] M. F. Rode, A. L. Sobolewski, *Chem. Phys.* **2012**, *409*, 41-48.

[18] a) J. Zhao, X. Liu, Y. Zheng, *J. Phys. Chem. A* **2017**, *121*, 4002-4008; b) R. Dutta, A. Pyne, D. Mondal, N. Sarkar, *ACS Omega* **2018**, *3*, 314-328; c) S. Mandal, S. Ghosh, C. Banerjee, J. Kuchlyan, N. Sarkar, *J. Phys. Chem. B* **2013**, *117*, 6789-6800; d) D. De, A. Datta, *J. Phys. Chem. B*, **2011**, *115*, 1032-1037.

[19] a) P. M. Vérité, C. A. Guido, D. Jacquemin, *Phys. Chem. Chem. Phys.* **2019**, *21* , 2307-2317; b) Y. Hao, Y. Chen, *Dyes Pigm.* **2016**, *129*, 186-190.

[20] S. Sahu, M. Das, A. K. Bhartia, G. Krishnamoorthy, *Phys. Chem. Chem. Phys.* **2018**, *20*, 27131-27139.

[21] H.-C. Chou, C.-H. Hsu, Y.-M. Cheng, C.-C. Cheng, H.-W. Liu, S.-C. Pu, P.-T. Chou, *J. Am. Chem. Soc.* **2004**, *126*, 1650-1651.

[22] X. Huang, J. Liu, J. Sheng, X. Song, Z. Du, M. Li, X. Zhang, Y. Zou, *Green Chem.* **2018**, *20*, 804.

10.1002/chem.202203116

WILEY-VCH

Entry for the Table of Contents

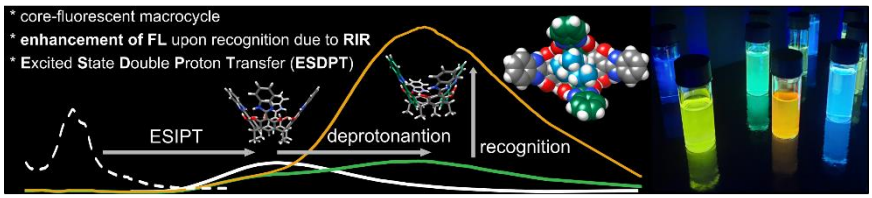

ESIPT-type resorcin[4]arenes are capable of guest-binding in the cavity and generate FL response with large Stokes shift and size-selective enhancement of emission via the mechanism that involves (a) selective di-deprotonation, (b) generation of emissive double keto tautomeric forms, and (c) recognition-induced restriction of intramolecular motion.

Institute and/or researcher Twitter usernames: @IOC_PAS